ACCOUNTS
of chemical research

Accurate Prediction of the Electronic Properties of Low-Dimensional Graphene Derivatives Using a Screened Hybrid Density Functional

VERONICA BARONE,[§,†] ODED HOD,[§,‡] JUAN E. PERALTA,[†] AND GUSTAVO E. SCUSERIA*[,¶]

[†]*Department of Physics, Central Michigan University, Mt. Pleasant, Michigan 48859, United States,* [‡]*Department of Chemical Physics, School of Chemistry, Tel Aviv University, Tel Aviv 69978, Israel, and* [¶]*Department of Chemistry and Department of Physics & Astronomy, Rice University, Houston, Texas 77005, United States*

RECEIVED ON OCTOBER 23, 2010

CONSPECTUS

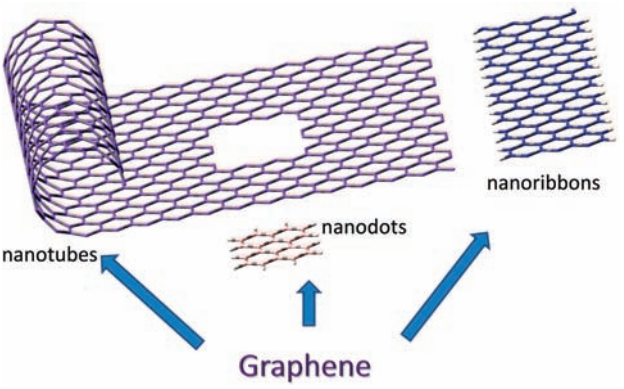

Over the last several years, low-dimensional graphene derivatives, such as carbon nanotubes and graphene nanoribbons, have played a central role in the pursuit of a plausible carbon-based nanotechnology. Their electronic properties can be either metallic or semiconducting depending purely on morphology, but predicting their electronic behavior has proven challenging. The combination of experimental efforts with modeling of these nanometer-scale structures has been instrumental in gaining insight into their physical and chemical properties and the processes involved at these scales. Particularly, approximations based on density functional theory have emerged as a successful computational tool for predicting the electronic structure of these materials. In this Account, we review our efforts in modeling graphitic nanostructures from first principles with hybrid density functionals, namely the Heyd−Scuseria−Ernzerhof (HSE) screened exchange hybrid and the hybrid meta-generalized functional of Tao, Perdew, Staroverov, and Scuseria (TPSSh).

These functionals provide a powerful tool for quantitatively studying structure−property relations and the effects of external perturbations such as chemical substitutions, electric and magnetic fields, and mechanical deformations on the electronic and magnetic properties of these low-dimensional carbon materials. We show how HSE and TPSSh successfully predict the electronic properties of these materials, providing a good description of their band structure and density of states, their work function, and their magnetic ordering in the cases in which magnetism arises. Moreover, these approximations are capable of successfully predicting optical transitions (first and higher order) in both metallic and semiconducting single-walled carbon nanotubes of various chiralities and diameters with impressive accuracy. This versatility includes the correct prediction of the trigonal warping splitting in metallic nanotubes.

The results predicted by HSE and TPSSh provide excellent agreement with existing photoluminescence and Rayleigh scattering spectroscopy experiments and Green's function-based methods for carbon nanotubes. This same methodology was utilized to predict the properties of other carbon nanomaterials, such as graphene nanoribbons. Graphene nanoribbons may be viewed as unrolled (and passivated) carbon nanotubes. However, the emergence of edges has a crucial impact on the electronic properties of graphene nanoribbons. Our calculations have shown that armchair nanoribbons are predicted to be nonmagnetic semiconductors with a band gap that oscillates with their width. In contrast, zigzag graphene nanoribbons are semiconducting with an electronic ground state that exhibits spin polarization localized at the edges of the carbon nanoribbon. The spatial symmetry of these magnetic states in graphene nanoribbons can give rise to a half-metallic behavior when a transverse external electric field is applied. Our work shows that these properties are enhanced upon different types of oxidation of the edges. We also discuss the properties of rectangular graphene flakes, which present spin polarization localized at the zigzag edges.

Published on the Web 03/09/2011 www.pubs.acs.org/accounts
10.1021/ar100137c

Introduction

Modeling the electronic properties of novel materials is an important goal of electronic structure methods. Successful methods must be accurate and at the same time computationally tractable so that they can be applied to large systems. Density functional theory (DFT) falls into this category, provided that the exchange and correlation functional (XC) is chosen adequately. There are many approximations for the choice of the XC functional in DFT calculations. Among the most widely used XC functionals are treatments that fall into the local(-spin) density approximation or L(S)DA and the generalized-gradient approximation or GGA. Examples are SVWN5, which consists of a combination of Dirac exchange and the parametrization of Vosko, Wilk, and Nusair for correlation, and the GGA functional of Perdew, Burke, and Ernzerhof (PBE) for exchange (see, for instance, ref 1). Comparing with experimental data, these functionals usually perform well for structural properties but present some limitations for energetics and electronic properties. More sophisticated XC functionals include an orbital dependency either through the kinetic energy density or the incorporation of Hartree−Fock (HF) type exchange.[1,2] Some realizations of these functionals include the meta-GGA of Tao, Perdew, Staroverov, and Scuseria[3] (TPSS), the hybrid functionals PBEh[1] (also known as PBE0), and the popular B3LYP.[1] These types of functionals usually show improvement over the LSDA and GGA but are computationally taxing. In particular, due to the slow decay of HF exchange in real space for small band gap semiconductors and metals, standard hybrid functionals can be computationally very demanding.[4] Short-range functionals, such as the screened hybrid functional of Heyd, Scuseria, and Ernzerhof[4] (HSE), have emerged as an efficient alternative to standard hybrid functionals. The HSE functional incorporates only the short-range portion instead of the full-range electron−electron interaction in the exchange contribution to the electronic energy. The computational advantage is that the short-range part of the HF exchange can be efficiently evaluated.[4] This truncation has little impact on the properties of finite systems while providing an efficient route for hybrid DFT calculations in extended systems.[5]

Exchange−correlation functionals, either originating from nonempirical grounds or using fitted parameters, are meant to approximate the electronic ground-state energy and not necessarily excited states. Kohn−Sham eigenvalues differences are regularly used to evaluate the fundamental energy band gap. While this is not a rigorous approach for regular semilocal DFT functionals, it is a valid alternative for hybrids whose generalized potential is of a nonlocal nature. In practice, Kohn−Sham eigenvalues are commonly used to discern between metals and semiconductors and to obtain excitation energies via linear response time-dependent DFT. LSDA and GGA band gaps underestimate experimental data as a rule, and even small-gap semiconductors can be erroneously predicted to be metallic. In contrast, band gaps obtained using hybrid functionals are, in general, in much better agreement with experimental data,[2,6,7] although somewhat overestimated. Screened hybrid functionals perform substantially better than regular hybrids for band gaps and provide excellent agreement with experiment and more rigorous many-electron approaches.[6,7] The rationale behind this success has been discussed in the literature,[8,9] and its elaboration is beyond the scope of this Account. We here only note that because of the nonlocal nature of the exchange potential in hybrids, band energy differences obtained with them are true band gaps (i.e., they include the "derivative discontinuity" missing in local Kohn−Sham approaches). Furthermore, excitation energies from time-dependent hybrid DFT approaches are an approximation to the Bethe−Salpeter equation and thus valid estimations of the optical response. Because of the short-range nature of the HSE potential, these excitation energies are very close to band energy differences in periodic systems.[8,9]

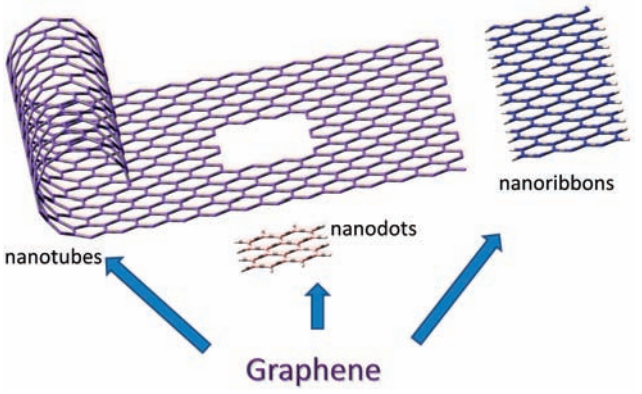

FIGURE 1. Schematic representation of some low-dimensional graphene derivatives.

Over the last several years, graphitic materials like carbon nanotubes and graphene nanoribbons (Figure 1) have played a central role for building a plausible carbon-based nanotechnology. This Account reviews our successful efforts in modeling from first principles the electronic properties of these nanostructures using hybrid density functionals, especially the HSE screened hybrid. Details of the calculations are given in the respective publications cited below. Calculations with periodic boundary conditions were done with

Gaussian orbitals and methods previously described in the literature.[10]

Single-Walled Carbon Nanotubes

The flexibility of the electronic properties of single-walled carbon nanotubes (SWNTs) has attracted much interest in the scientific community. These tubular materials can be either metallic or semiconducting depending strictly on their morphology, that is, their diameter and chirality. Predicting their electronic behavior and optical properties accurately has proven to be a challenging task for most electronic structure methods. Methods based on the tight-binding approach miss some important curvature effects, while sophisticated many-body approaches are costly in terms of computational resources, especially in the case of chiral SWNTs, containing many atoms in the translational unit cell. DFT methods have thus been employed as a computationally efficient choice for obtaining the electronic structure of SWNTs. However, as mentioned above, conventional semilocal functionals present considerable problems describing quantitatively the band gap of semiconducting materials. These problems can be circumvented by hybrid functionals. In our work, the screened exchange hybrid HSE and the hybrid meta-generalized gradient approximation TPSSh, were shown to accurately reproduce and predict the electronic structure of SWNTs.[6,7,11]

A nice illustration of all these complex features is found in the study of narrow SWNTs. For instance, the (5,0) SWNT, which should be a semiconductor according to the zone folding scheme, is predicted to be metallic by DFT calculations.[11−13] The same holds true for the zigzag (4,0) SWNT.[11,12] Although it is appealing to assume that narrower tubes are metallic due to a strong $\sigma-\pi$ hybridization, it has been shown that the narrowest chiral tubes present the largest band gaps of all SWNTs. These band gaps can be as large as 1.7 eV for the (4,3) tube (obtained using the HSE functional).[11] These strong curvature effects transform narrow semiconducting SWNTs into indirect gap semiconductors that abruptly deviate from the zone folding predictions. As shown in Figure 2 for the (4,2) tube, the calculated electronic properties of narrow nanotubes strongly depend on the exchange−correlation functional utilized in the calculations. LSDA predicts a small band gap of about 0.20 eV for this tube, while the hybrids HSE and PBEh predict a larger band gap of 0.74 and 1.36 eV, respectively. This follows a more general trend where the band gap of SWNTs is severely underestimated by LSDA and considerably overestimated by PBEh whereas HSE values are, in general, in excellent agreement with experiments.[6]

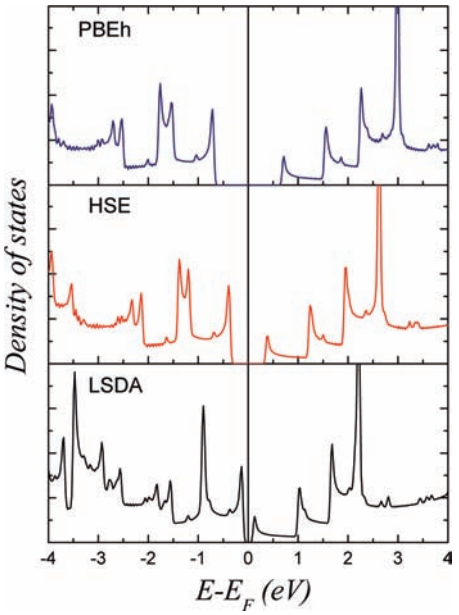

FIGURE 2. Density of states for the chiral semiconducting (4,2) nanotube obtained with LSDA, HSE, and PBEh.

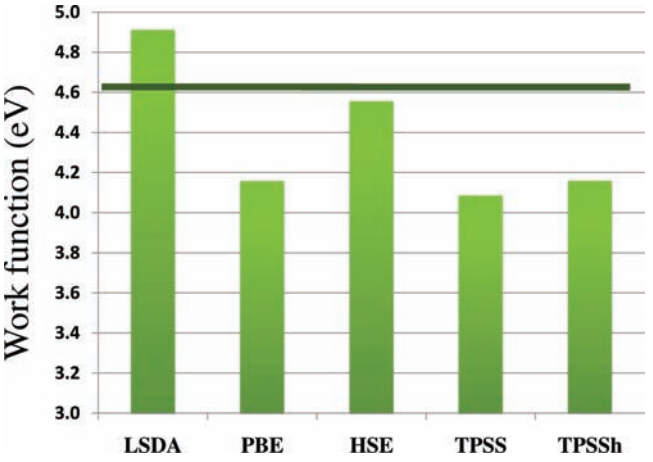

FIGURE 3. Work function of graphene calculated using different functionals. The experimental value for graphite is 4.6 eV (horizontal line).[14]

Another fundamental electronic property related to the electron field emission of SWNTs is their work function (WF).[14] An accurate prediction of the ground state is needed to obtain the work function of SWNTs. Similar to the case of band gap calculations, this condition imposes a stringent requirement on the choice of approximate density functional. This requirement is fulfilled by the HSE functional because it provides the most accurate prediction of the WF of graphene as shown in Figure 3. Calculations of the WF in a set of metallic and semiconducting tubes with different chiralities and diameters performed with the HSE functional predict that SWNTs with diameters larger than 0.9 nm tend asymptotically to the graphene limit of 4.6 eV irrespective of their electronic

behavior. This does not hold true for narrow nanotubes because their WF exhibits a significant dependence on their diameter and chiral angle, which has been attributed to strong hybridization effects induced by curvature.[14]

Despite all these interesting results, it is in the prediction of SWNTs optical properties where HSE and TPSSh provide the most outstanding results.[6,7] Optical transitions in individual SWNTs have been determined by a variety of experiments.[15,16] These transitions represent a fingerprint of a given nanotube that unequivocally relates its diameter and chirality with its electronic properties, providing a rigorous test for theoretical models attempting to predict these properties. Early theoretical studies of optical transitions in SWNTs were performed using the tight-binding approximation and considering excitations as interband transitions. Within this approach, the optical spectrum is obtained employing the random-phase approximation (RPA) for the imaginary part of the dielectric function ε as

$$\mathrm{Im}(\varepsilon) = \frac{1}{\omega^2}\sum_{\mathbf{k}}\sum_{\mathrm{o,u}} |\langle\psi_{\mathrm{o}}^{\mathbf{k}}|\mathbf{p}|\psi_{\mathrm{u}}^{\mathbf{k}}\rangle|^2 \delta(\varepsilon_{\mathrm{o}}^{\mathbf{k}} - \varepsilon_{\mathrm{u}}^{\mathbf{k}} - \omega) \qquad (1)$$

where **p** is the linear momentum operator and the indices o and u stand for occupied and unoccupied Bloch orbitals, respectively.

The first experiments using photoluminescence provided accurate values for the optical gap in semiconducting nanotubes and a valuable test set of moderately large unit cells tubes (ranging from a few tens to more than 500 carbon atoms) where optical transitions could be evaluated using different DFT approaches and RPA.[6,15] Within this approach, the optical gap is then equivalent to the fundamental band gap obtained as band energy differences provided that the transitions are dipole-allowed. Barone et al.[6] have shown that the band gap of semiconducting tubes is not sensitive to the level of geometry optimization. This allows for the utilization of simple functionals (such as LSDA) and a modest Gaussian basis set such as STO-3G to perform geometry optimizations in semiconducting tubes thus significantly reducing the computational effort, especially in large unit cell chiral SWNTs. Further geometry optimizations using other functionals and basis sets produce a rather small change in the band gaps, typically smaller than 1%.[6] Undoubtedly, the main factor impacting the quality of the band gap calculations within the DFT approximation is the choice of the density functional. This is well demonstrated in Figure 4 where the mean errors of the optical gap in a set of ten semiconducting tubes are presented for different density functionals. We observed the well-known trend that nonhybrid functionals underestimate

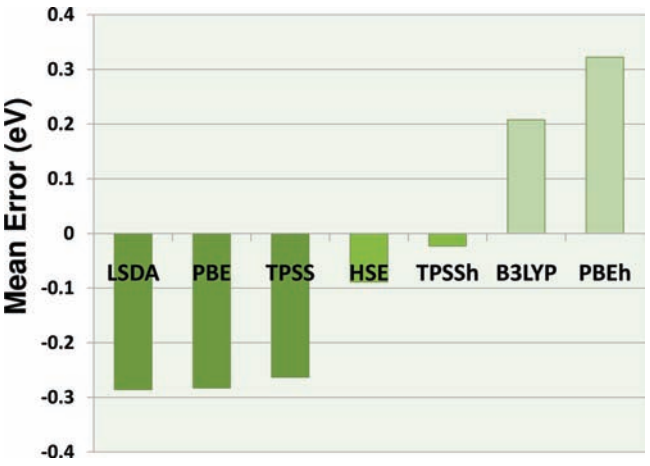

FIGURE 4. Mean errors for the first optical transition (in eV) in a set of ten semiconducting tubes for different density functionals.

the experimental band gap. On the other hand, the hybrid PBEh and B3LYP functionals overestimate band gaps by about 0.3 eV. The performance of HSE is much better; it presents absolute errors smaller than 0.10 eV. TPSSh improves the agreement with experiment even further with deviations that are in all cases less than 0.05 eV.

The success of these hybrid functionals transcends the optical gap of semiconducting tubes. Using the same formalism, one can obtain higher order optical transitions (denoted herein as E_{ii}, where i refers to the order of the dipole allowed transition between the ith valence band and the ith conduction band) that have also been experimentally measured by Bachilo et al.[15] TPSSh results are presented together with experimental values in a large set of tubes in Figure 5. We note that the excellent agreement obtained for the first transitions (optical gap) is also found for second-order transitions. Theoretically predicted third- and fourth-order transitions present larger deviations with respect to the experimental assignments but fit quite well the range of the available experimental values.

These noteworthy results lead to the question of how would HSE and TPSSh perform for metallic tubes since the Hartree−Fock approximation presents serious deficiencies for describing the metallic behavior of bulk materials. In Figure 6, we present the calculated first optical transitions of five metallic and five semiconducting tubes obtained using different functionals.[7] Nonhybrid functionals still underestimate E_{11} in metallic tubes, while in this case, HSE and TPSSh perform similarly and present small deviations with respect to the experimental values. Calculations performed with other hybrid functionals as B3LYP or PBEh pose severe convergence problems for these metallic tubes and are therefore not included in the plot.[7]

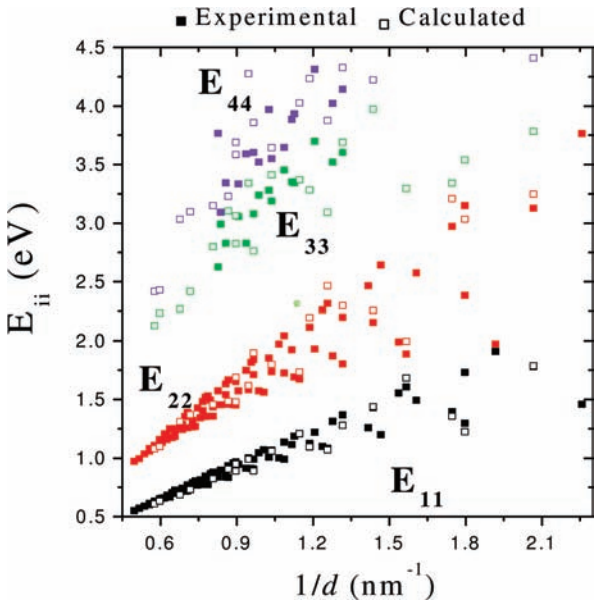

FIGURE 5. Optical transitions of semiconducting SWNTs as a function of the inverse diameter. Filled symbols represent experimentally assigned values while open symbols are calculated values.[6]

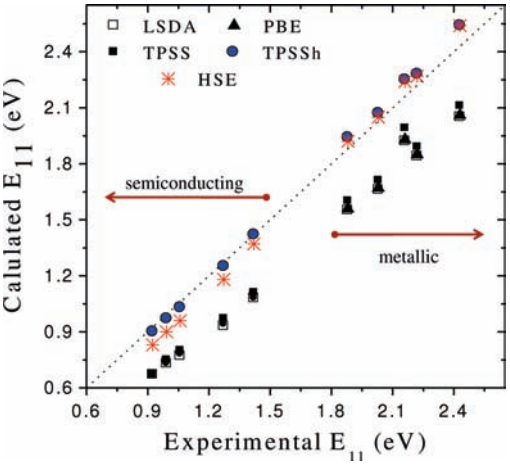

FIGURE 6. First optical transition in a set of five semiconducting and five metallic nanotubes obtained with different density functionals.

Metallic tubes other than armchairs exhibit a splitting of the van Hove singularities due to the trigonal warping effect.[17,18] This splitting separates the electronic transitions in zigzag and chiral *metallic* SWNTs in a lower (E_{11}^{-}) and an upper (E_{11}^{+}) branches with respect to the armchair curve. Results obtained with both HSE and TPSSh for the trigonal warping splitting are about twice as large as the ones predicted by the zone-folding scheme.[7] This larger-than-expected splitting predicted by hybrid functionals could provide an explanation of why the upper branches were not observed in some experiments in which they were searched using a narrow laser window while expecting a smaller splitting.[16] Indeed, later experiments based on Rayleigh scattering spectroscopy[19] have proven that our predicted values for the lower and upper branches in metallic tubes are exceptionally accurate, as shown in Table 1.

TABLE 1. Lower Optical Transitions (in eV) in Metallic SWNTs Calculated Using the TPSSh and HSE Functionals[7] Compared with Experiments Based on Rayleigh Scattering Spectroscopy[19]

tube	transition	HSE	TPSSh	exp
(10,10)	E_{11} (no split)	1.86	1.89	1.93
(11,8)	E_{11}^{-}	1.91	1.92	1.93
(11,8)	E_{11}^{+}	1.99	2.02	2.02

TABLE 2. First-Order Optical Transitions (eV) in Metallic and Semiconducting Tubes Calculated Using the Hybrid TPSSh and HSE Functionals and GW Plus Electron−Hole Interactions (GW + e−h)

tube	TPSSh[6,7]	HSE[6,7]	GW + e−h[20]
	Semiconductor		
(10,0)	1.04	0.97	1.00
(11,0)	1.19	1.12	1.21
	Metallic		
(12,0)	2.25	2.24	2.25
(10,10)	1.89	1.86	1.84

Calculations beyond mean field theory have shown the excitonic nature of optical transitions in SWNTs with large exciton binding energies (of up to 1 eV for the (8,0) SWNT).[20] In Table 2, we compare first-order transitions calculated using the TPSSh and HSE functionals and calculations considering GW plus electron−hole interactions (GW + e−h).[20] It is worth pointing out that the results obtained with these functionals predict peak positions in excellent agreement with more complex quasi-particle and excitonic effects approaches. A phenomenological rationalization for this behavior has been presented by Brothers et al.[8]

Graphene Nanoribbons

Experimental and computational studies of graphene, a two-dimensional and atomically thin layer of graphite, and its lower-dimensional derivatives have grown exponentially in the past few years since high-quality graphene preparation was first reported by Novoselov and Geim in 2004.[21] When a graphene sheet is rolled to form a single-walled carbon nanotube (SWNT), the π electrons become confined along the circumferential direction obeying periodic boundary conditions. If instead the sheet is cut to form a graphene nanoribbon (GNR) of nanometer scale width and infinite length, "particle in a ring" type boundary conditions are replaced by "particle in a box" confinement in the direction perpendicular to the ribbon's axis. This quantum confinement of the π electrons results in a discrete set of allowed

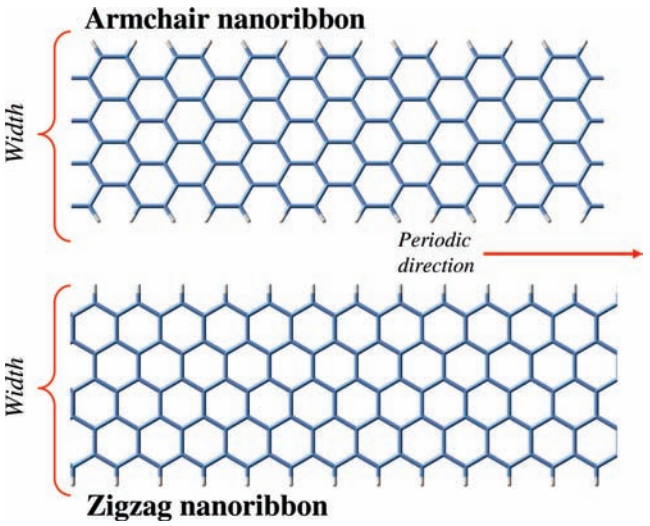

FIGURE 7. A schematic representation of armchair and zigzag graphene nanoribbons.

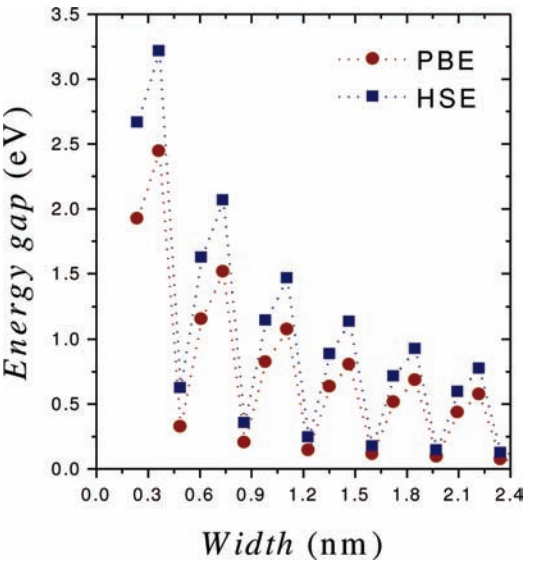

FIGURE 8. Width-dependent band gap oscillations of AGNRs showing 3-fold periodicity as calculated using the PBE and HSE functional approximations.[24]

energy bands slicing the otherwise continuous two-dimensional dispersion surface of graphene. As the width of the ribbon (or diameter of the nanotube) is varied, the number and position of the allowed bands in the reciprocal space changes inducing size-dependent band gap variations.

Structurally, graphene nanoribbons may be viewed as unrolled (and passivated) carbon nanotubes. One may naively deduce that the electronic properties of the unrolled nanoribbon are similar to those of the original nanotube. Nevertheless, a major difference between the two systems arises: when the tube is unrolled, new edges are exposed which may have a crucial impact on the electronic properties of the resulting nanoribbon.

We start here discussing the case of armchair graphene nanoribbons (AGNRs), which similar to the case of zigzag SWNTs, are expected to show large band gap variations as a function of the ribbon's width (see Figure 7). Based on tight-binding (TB) calculations, it was deduced that such band gap variations do exist obeying a 3-fold periodic pattern with every third ribbon width showing a metallic character.[22]

Interestingly, when higher level DFT calculations are performed based on LSDA,[23] PBE, and the HSE screened-exchange hybrid functional, the band gap oscillations prevail (see Figure 8); however, all AGNRs are predicted to be semiconducting.[24] This is in stark contrast to the case of zigzag SWNTs where a third of the tubes are found to be metallic.

As one may expect, the amplitude of the predicted band gap oscillations depends on the functional approximation used. Nevertheless, the general periodicity and the fact that all AGNRs are semiconducting is consistent within all the calculations, exemplifying the influence of the edges on the electronic structure of the system. Thus far, the theoretically predicted dependence of the band gap on the exact width of the nanoribbon has not been observed experimentally.

Nonetheless, recent experimental band gap measurements have reported good agreement with predictions obtained via density functional theory calculations.[25] Interestingly, Avouris et al.[26] have found good agreement with results obtained using the HSE functional whereas Dai et al.[27] found better agreement with LSDA results. This discrepancy may be related to the uncertainty in the determination of the ribbons' width, especially for the narrower ribbons measured.[27] Advances in ultrathin nanoribbon fabrication and synthesis may shed light on this issue as well as open the way to accurate control over their electronic properties.[28]

When the length of an AGNR is taken to be finite, a rectangular graphene nanodot is formed. If the width and length of such dot are both in the nanoscale regime, the resulting system will have a molecular character. Coming from the two-dimensional (2D) crystal point of view, the additional confinement of the π electrons has a considerable influence over the electronic properties of the nanodot.[29] In Figure 9, the molecular HOMO−LUMO gap is presented as a function of the lateral and longitudinal dimensions for a large set of rectangular graphene nanodots. Here, results obtained by the LSDA (upper left panel), PBE (upper right panel), and HSE (lower left panel) are given. The studied nanodots are denoted by $N \times M$ where N (M) is the number of

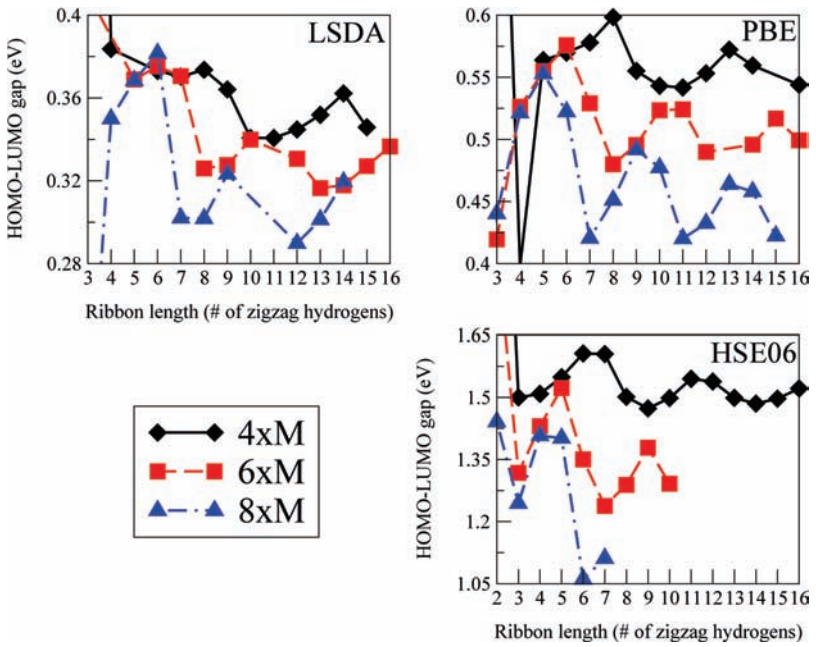

FIGURE 9. HOMO−LUMO gap variations as a function of graphene nanodot dimensions calculated by the local spin density approximation (upper left panel), PBE functional (upper right panel), and the HSE functional (lower right panel).

hydrogen atoms passivating each armchair (zigzag) edge. As can be seen, oscillatory variations of the band gap as a function of the dimensions of the nanodots are obtained, though their amplitude is smaller compared with the case of infinite AGNRs. Naturally, as *N* is increased, the armchair edge is elongated and the oscillation amplitude increases approaching the infinite AGNRs case. The 3-fold periodicity is not apparent for the quasi-zero-dimensional system because the changes in width have to be done in larger quanta in order to prevent the formation of dangling edge bonds. For the systems studied, when the calculation is performed using LSDA, the calculated band gap values are on the order of 0.3−0.4 eV. Slightly larger values (0.4−0.6 eV) are obtained when the generalized gradient approximation is used within the semilocal PBE functional. The screened-exchange HSE functional predicts band gaps in the range of 1.0−1.6 eV.

Despite the differences between the functional approximations, a general trend is identified, one where the HOMO−LUMO gaps become smaller as the dimensions of the nanodot are increased. This is consistent with the naive "particle in a two dimensional box" picture and with the semimetallic nature of the infinite graphene layer. Therefore, the dimensions of the graphene nanodot may be used as a control parameter to tune the electronic nature of the system. Here, elongated armchair edges and nanoscale zigzag edges are desirable, resulting in large band gap variations and enhanced control capabilities.

As discussed above, the appearance of exposed edges in graphene nanoribbons may have a crucial effect on their electronic properties. One of the most interesting systems exemplifying this characteristic are zigzag graphene nanoribbons (ZZGNRs) (see Figure 7). There, apart from the quantum confinement effects discussed above, considerable edge states appear to be localized at the zigzag edges. The existence of such states, which have been theoretically related to the unique geometry of the hexagonal lattice and its zigzag edges,[30] has been recently verified experimentally.[31] While standard conjugated organic molecules are considered to be nonmagnetic, theoretical treatments predict that these edge states induce a spin-polarized ground state for ZZGNRs.[30,32]

Similar to the case of AGNRs, one may view ZGNRs as unrolled armchair SWNTs. Here, the difference in the electronic character between the two systems is pronounced. Within closed shell DFT calculations, all ZZGNRs turn out to be metallic.[32] However, if the spin degree of freedom is taken into account (via an unrestricted Kohn−Sham scheme), the ground state of the system becomes spin-polarized with one zigzag edge carrying one spin flavor and the other edge carrying the opposite spin. This long-range antiparallel spatial spin distribution may be rationalized via Clar's sextet theory[33] and is a result of antiferromagnetic spin ordering on adjacent carbon sites of the graphene hexagonal lattice. The resulting ground state of

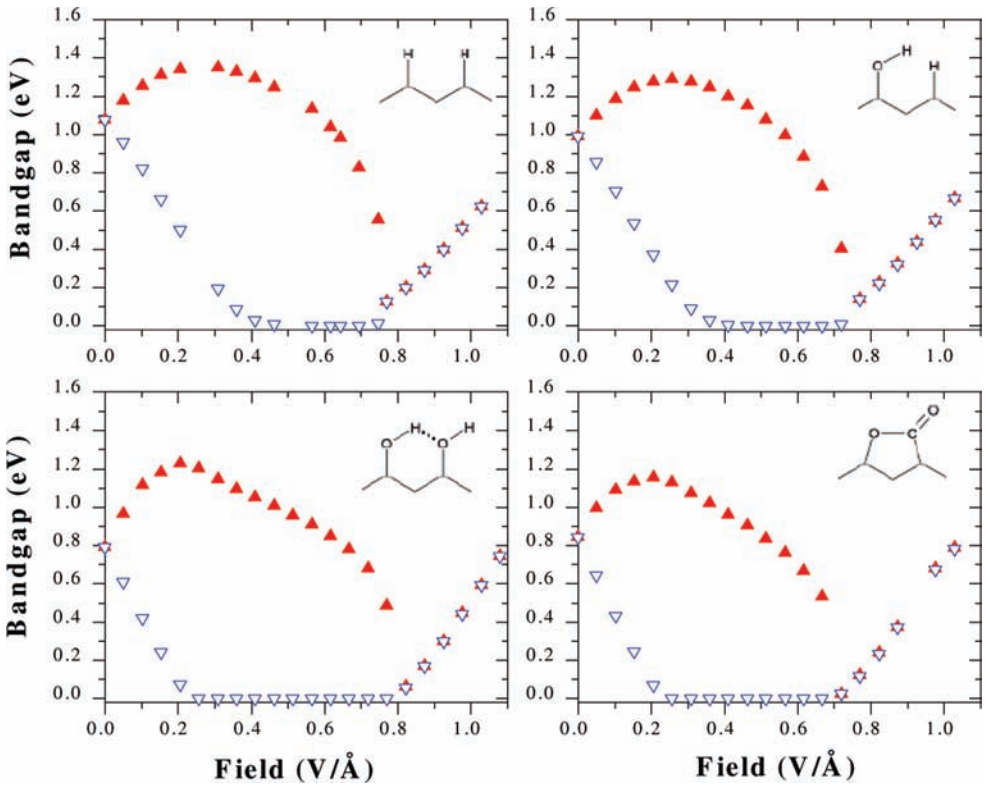

FIGURE 10. Electric field effect on the spin-polarized band gap of oxidized GNRs as calculated using the HSE functional. Red and blue triangles stand for the two different spin polarization band gaps.

all ZZGNRs is found to be semiconducting in stark contrast to the metallic nature of the corresponding armchair SWNTs.[32]

The unique spatial symmetry of the magnetic zigzag edge states in graphene allows for interesting interplay between the electronic and magnetic properties of the system. With DFT calculations, it was recently shown that by applying an in-plane electric field perpendicular to the ribbon's axis, one may separately control the band gaps associated with the two spin flavors up to a point where the system becomes half-metallic.[32] The mechanism responsible for this effect relates to the accumulation of positive and negative charges along the two opposing zigzag edges. This charge induces local gating of opposite sign that shifts the spin polarized local density of states of one edge with respect to the other. As a result, the band gap associated with one spin polarization is increased, while the opposite spin band gap decreases. At a large enough electric field intensity, the decreasing band gap vanishes thus achieving a half-metallic state. At this point, an electron approaching the system with one spin polarization will experience a metallic behavior, whereas an electron with the opposite spin will see a semiconductor behavior. Therefore, this state could be used as a spin filter that is a crucial component of any future nanoscale spintronic device.

From what we have seen thus far, it is clear that edge states have an important role in dictating the electronic properties of GNRs. Based on this observation, it was suggested that edge chemistry may be used to control the electronic character of ZZGNRs. Since most of graphene device fabrication is performed in standard laboratory conditions, one should expect that the reactive zigzag edge dangling bonds will bond to oxygen-containing groups. An interesting question arises in this respect regarding the robustness of the half-metallic state of graphene toward the chemical modification of the zigzag edges. In order to address this question, a DFT study based on the screened-exchange HSE[4] functional approximation was conducted with results showing enhanced stability toward most edge oxidation schemes.[34] Interestingly, the stable oxidized molecules have a spin-polarized electronic ground state with an antiparallel spin alignment on the two zigzag edges similar to the hydrogenated ZZGNRs discussed above.

Once the stability of the oxidized systems has been established, it is possible to check the influence of edge chemistry on the existence of the half-metallic state. Figure 10 presents the spin-resolved band gaps of the oxidized systems as a function of the electric field intensity compared with the behavior of the fully hydrogenated

ZZGNR. All the systems considered present a similar behavior where both spin-polarized band gaps are degenerate in the unperturbed system. Once the electric field is turned on, the band gaps split with one spin channel presenting an increased gap and the opposite spin channel showing a decreased gap. As discussed above, at a large enough electric field, the band gap of one of the channels vanishes thus achieving a half-metallic state. Upon further increase in the external field's intensity, spin-polarized charge transfer between the two edges induces spin compensation that results in a reduction of the band gap splitting until they become degenerate and a nonmagnetic state is obtained.

An important difference is identified between the response of the hydrogenated (fully and partially) systems and that of the fully oxidized systems to the application of the external electric field. In the case of the hydrogenated systems, the onset electric field intensity required to turn the studied systems half-metallic is 0.4 V/Å with an operative range (the range at which the half-metallic state is obtained) of 0.3 V/Å. Upon full oxidation of the zigzag edges, the half-metallic state is obtained already at a field of 0.2 V/Å and sustains up to a field of 0.8 V/Å. This decrease in onset field intensity and increase in operative range marks edge oxidation as an important tool for achieving chemically stable and robust spin filters based on ZZGNRs. Though more challenging experimentally, selective edge chemistry with the attachment of groups of different electronegativity to the two edges has been predicted to induce a half-metallic ground state with no external field.[35]

As stated above, it is commonly accepted that standard conjugated organic molecules such as polyaromatic hydrocarbons are nonmagnetic in their ground electronic state. Nevertheless, in the limit of infinite zigzag edges, ZGNRs have a spin-polarized ground state. It is therefore interesting to study the minimal length at which finite rectangular graphene quantum dots present a spin-polarized ground state. Theoretical studies using Huckel theory have addressed this issue long before the first experimental realization of graphene nanoribbons. These studies showed that finite zigzag edges of graphene flakes exhibit a spin-polarized ground state.[36] Recently, several theoretical studies have revisited this issue considering finite graphitic systems such as rectangular[29,37] and triangular[38] graphene flakes, as well as finite zigzag SWNT segments.[39]

For the case of rectangular graphene flakes, DFT calculations using a variety of functional approximations (including HSE, B3LYP, and PBEh) predicted that even very small molecular derivatives of graphene, such as $C_{36}H_{16}$

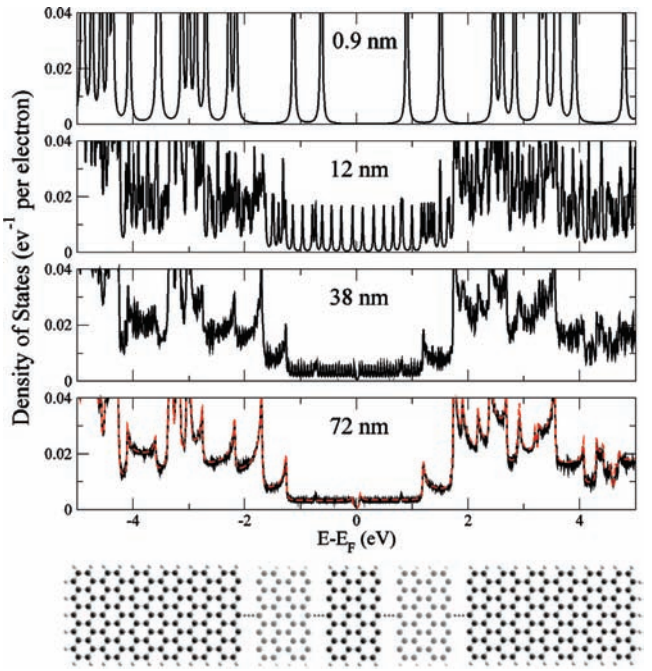

FIGURE 11. Lower panel, a schematic representation of a finite elongated graphene nanoribbon. Upper panels, DOS of finite GNRs as a function of their length. The dashed red curve in the lowermost DOS panel is the DOS of the infinite system.[41]

(tetrabenzo[*bc*,*ef*,*kl*,*no*]coronene) and the bisanthrene (phenanthro[1,10,9,8-*opqra*]perylene) isomer of $C_{28}H_{14}$, have a spin-polarized ground state.[29,37] This has been further validated via complete active space self-consistent field wave function calculations.[37] When an electric field is applied perpendicular to the zigzag edge within the molecular plane, the finite flakes reach a half-metallic state where the HOMO−LUMO gap of one spin flavor vanishes and the gap of the opposite spin flavor increases with the field intensity.[29] The same behavior was predicted based on DFT calculations for finite segments of zigzag SWNTs.[39]

When considering triangular graphene flakes with pure zigzag edges, one finds that spin frustration leads to a ground electronic state bearing a permanent magnetic moment.[38] This is a result of the unique tailoring of the zigzag edges at the triangle corners together with the antiferromagnetic spin ordering within the hexagonal carbon lattice. These results, which were obtained via the Hubbard model and GGA based DFT calculations, were shown to be consistent with Lieb's theorm for the total spin of the ground state of bipartite lattices.[38] Therefore, triangular graphene flakes, in which the zigzag edges bear a large magnetic moment, may be viewed as promising molecular magnets for future nanoelectronic, nanospintronic, and memory devices.

An interesting question that may arise regards the influence of the localized edge states on the electronic properties of the full system as a function of its dimensions. Figure 11 presents the DOS of a set of graphene nanoribbons of constant width and increasing length (see lower panel of the figure) calculated using a recently developed divide-and-conquer (D&C) approach[40] within the HSE exchange–correlation functional approximation. For short ribbons (see upper panels), the DOS resembles that of a molecular system consisting of discrete energy levels. As the length of the ribbon is increased to 38 nm, typical features of the DOS of infinite systems, such as the van Hove singularities and the finite density of states in the vicinity of the Fermi energy, start to develop. The DOS of a 72 nm length GNR is already in excellent agreement with that of the infinite system where most of the features related to edge states almost completely vanish. Results obtained for other GNRs of different widths[41] show that the scaling of the effects of edge states with the length depends on the electronic character of the underlying system. As exemplified here, the D&C approach is a powerful method for performing electronic structure and transport calculations of extremely large molecular systems using advanced DFT functional approximations.

Final Remarks

As shown in this Account, two-dimensional graphene and its lower dimensional derivatives span a diverse collection of electronic properties. These range from *semimetallic* graphene, through *semiconducting* SWNTs and GNRs, *metallic* SWNTs, and *half-metallic* zigzag GNRs and finite zigzag nanotube segments. Simplified approaches based on model Hamiltonians may yield important insights on their general physical trends. Nevertheless, DFT, in general, and the HSE screened hybrid approximation, in particular, provide excellent tools for quantitatively studying structure–function relations and the effects of external perturbations such as chemical substitutions,[42,43] electric and magnetic fields, and mechanical deformations.[44] Moreover, to study the properties of novel carbon materials such as the biphenyl sheet and its one-dimensional derivatives,[45] the utilization of HSE is critical in order to obtain not only the correct electronic behavior but also quantitatively accurate band gaps.

V.B. acknowledges the donors of the American Chemical Society Petroleum Research Fund for support of this research through Award No. ACS PRF 49427-UNI6. O.H. acknowledges the support of the Israel Science Foundation under Grant No. 1313/08, the support of the Center for Nanoscience and Nanotechnology at Tel-Aviv University, and the Lise Meitner-Minerva Center for Computational Quantum Chemistry. The research leading to these results has received funding from the European Community's Seventh Framework Programme FP7/2007-2013 under Grant Agreement 249225. J.E.P. acknowledges support from NSF DMR-0906617. The work at Rice University was supported by NSF CHE-0807194, DOE Grants DE-FG02-04ER15523 and DE-FG02-09ER16053, and the Welch Foundation C-0036.

BIOGRAPHICAL INFORMATION

Veronica Barone earned her undergraduate degree (2000) and Ph.D. (2003) in physics from the University of Buenos Aires (Argentina). After a postdoctoral work at Rice University, she joined the Physics Department at Central Michigan University as an Assistant Professor. During the past seven years, her work has focused on understanding, using density functional theory, the chemical and physical properties of low-dimensional carbon materials for technological applications.

Oded Hod received his B.Sc. from the Hebrew University (1994) and his Ph.D. from Tel-Aviv University (2005). After completing a postdoctoral term at Rice University, he joined Tel Aviv University in 2008. His research involves computational nanomaterials science including electronic structure, mechanical and electromechanical properties, density functional theory, molecular electronics, and electron dynamics in open quantum systems.

Juan E. Peralta graduated from the University of Buenos Aires (Argentina) in 1997 and completed his Ph.D. in physics from the same institution in 2002. After five years as a postdoctoral researcher at Rice University, he joined the Physics Department at Central Michigan University as an Assistant Professor in 2007. His current work focuses on the computational modeling of magnetic materials with density functional theory.

Gustavo E. Scuseria is the Robert A. Welch Professor of Chemistry and Professor of Physics and Astronomy at Rice University. During the last 25 years, his research group has pioneered methodologies for coupled cluster theory, linear scaling electronic structure methods, and density functional theory with applications to carbon nanosystems and solid state.

FOOTNOTES

*To whom correspondence should be addressed. E-mail: guscus@rice.edu.
§ These authors contributed equally to this work.

REFERENCES

1 Scuseria, G. E. Staroverov, V. N, Development of approximate exchange-correlation functionals. In *Theory and Applications of Computational Chemistry: The First 40 years*; Dykstra, C. E., Frenking, G., Kim, K. S., Scuseria, G. E., Eds.; Elsevier: 2005; Chapter 24, pp 669–724.

2 Kümmel, S.; Kronik, L. Orbital-dependent density functionals: Theory and applications. *Rev. Mod. Phys.* **2008**, *80*, 3–60.

3 Tao, J.; Perdew, J. P.; Staroverov, V. N.; Scuseria, G. E. Climbing the density functional ladder: nonempirical meta-generalized gradient approximation designed for molecules and solids. *Phys. Rev. Lett.* **2003**, *91*, No. 146401.

4 Heyd, J.; Scuseria, G. E.; Ernzerhof, M. Hybrid functionals based on a screened Coulomb potential. *J. Chem. Phys.* **2003**, *118*, 8207–8215.

5 Heyd, J.; Scuseria, G. E. Efficient hybrid density functional calculations in solids: Assessment of the Heyd-Scuseria-Ernzerhof screened Coulomb hybrid functional. *J. Chem. Phys.* **2004**, *121*, 1187–1192.

6 Barone, V.; Peralta, J. E.; Wert, M.; Heyd, J.; Scuseria, G. E. Density functional theory study of optical transitions in semiconducting single-walled carbon nanotubes. *Nano Lett.* **2005**, *5*, 1621–1624.

7 Barone, V.; Peralta, J. E.; Scuseria, G. E. Optical transitions in metallic single-walled carbon nanotubes. *Nano Lett.* **2005**, *5*, 1830–1833.

8 Brothers, E. N.; Izmaylov, A. F.; Normand, J. O.; Barone, V.; Scuseria, G. E. Accurate solid-state band gaps via screened hybrid electronic structure calculations. *J. Chem. Phys.* **2008**, *129*, No. 011102.

9 Izmaylov, A. F.; Scuseria, G. E. Why are time-dependent density functional theory excitations in solids equal to band structure energy gaps for semilocal functionals, and how does nonlocal Hartree-Fock type exchange introduce excitonic effects? *J. Chem. Phys.* **2008**, *129*, No. 034101.

10 Kudin, K. N.; Scuseria, G. E. Linear scaling density functional theory with Gaussian orbitals and periodic boundary conditions: Efficient evaluation of energy and forces via the fast multipole method. *Phys. Rev. B* **2000**, *61*, 16440–16453.

11 Barone, V.; Scuseria, G. E. Theoretical study of the electronic properties of narrow singlewalled carbon nanotubes: Beyond the local density approximation. *J. Chem. Phys.* **2004**, *121*, 10376–10379.

12 Cabria, I.; Mintmire, J. W.; White, C. T. Metallic and semiconducting narrow carbon nanotubes. *Phys. Rev. B* **2003**, *67*, No. 121406.

13 Machón, M.; Reich, S.; Thomsen, C.; Sánchez-Portal, D.; Ordejón, P. Ab initio calculations of the optical properties of 4-angstrom-diameter single-walled nanotubes. *Phys. Rev. B* **2002**, *66*, No. 155410.

14 Barone, V.; Peralta, J. E.; Uddin, J.; Scuseria, G. E. Screened exchange hybrid density functional study of the work function of pristine and doped single-walled carbon nanotubes. *J. Chem. Phys.* **2006**, *124*, No. 024709.

15 Bachilo, S. M.; Strano, M. S.; Kittrell, C.; Hauge, R. H.; Smalley, R. E.; Weisman, R. B. Structure-assigned optical spectra of single-walled carbon nanotubes. *Science* **2002**, *298*, 2361–2366.

16 Fantini, C.; Jorio, A.; Souza, M.; Strano, M. S.; Dresselhaus, M. S.; Pimenta, M. A. Optical transition energies for carbon nanotubes from resonant Raman spectroscopy: Environment and temperature effects. *Phys. Rev. Lett.* **2004**, *93*, No. 147406.

17 Mintmire, J.; White, C. Universal density of states for carbon nanotubes. *Phys. Rev. Lett.* **1998**, *81*, 2506–2509.

18 Reich, S.; Thompsen, C. Chirality dependence of the density-of-states singularities in carbon nanotubes. *Phys. Rev. B* **2000**, *62*, 4273–4276.

19 Sfeir, M. Y.; Beetz, T.; Wang, F.; Huang, L. M.; Huang, X. M. H.; Huang, M. Y.; Hone, J.; O'Brien, S.; Misewich, J. A.; Heinz, T. F.; Wu, L. J.; YM, Y. M. Z.; Brus, L. E. Optical spectroscopy of individual single-walled carbon nanotubes of defined chiral structure. *Science* **2006**, *312*, 554–556.

20 Spataru, C. D.; Ismael-Beigi, S.; Capaz, R. B.; Louie, S. G. Quasiparticle and excitonic effects in the optical response of nanotubes and nanoribbons. *Top. Appl. Phys.* **2008**, *111*, 195–227.

21 Novoselov, K. S.; Geim, A. K.; Morozov, S. V.; Jiang, D.; Zhang, Y.; Dubonos, S. V.; Grigorieva, I. V.; Firsov, A. A. Electric field effect in atomically thin carbon films. *Science* **2004**, *306*, 666–669.

22 Ezawa, M. Peculiar width dependence of the electronic properties of carbon nanoribbons. *Phys. Rev. B* **2006**, *73*, No. 045432.

23 Son, Y.-W.; Cohen, M. L.; Louie, S. G. Energy gaps in graphene nanoribbons. *Phys. Rev. Lett.* **2006**, *97*, No. 216803.

24 Barone, V.; Hod, O.; Scuseria, G. E. Electronic structure and stability of semiconducting graphene nanoribbons. *Nano Lett.* **2006**, *6*, 2748–2754.

25 Han, M. Y.; Oezyilmaz, B.; Zhang, Y.; Kim, P. Energy band-gap engineering of graphene nanoribbons. *Phys. Rev. Lett.* **2007**, *98*, No. 206805.

26 Chen, Z.; Lin, Y.-M.; Rooks, M. J.; Avouris, P. Graphene nano-ribbon electronics. *Physica E* **2007**, *40*, 228–232.

27 Li, X.; Wang, X.; Zhang, L.; Lee, S.; Dai, H. Chemically derived, ultrasmooth graphene nanoribbon semiconductors. *Science* **2008**, *319*, 1229–1232.

28 Cai, J.; Ruffieux, P.; Jaafar, R.; Bieri, M.; Braun, T.; Blankenburg, S.; Muoth, M.; Seitsonen, A. P.; Saleh, M.; Feng, X.; Müllen, K.; Faselroman, R. Atomically precise bottom-up fabrication of graphene nanoribbons. *Nature* **2010**, *466*, 470–473 and references therein.

29 Hod, O.; Barone, V.; Scuseria, G. E. Half-metallic graphene nanodots: A comprehensive firstprinciples theoretical study. *Phys. Rev. B* **2008**, *77*, No. 035411 and references therein.

30 Fujita, M.; Wakabayashi, K.; Nakada, K.; Kusakabe, K. Peculiar localized state at zigzag graphite edge. *J. Phys. Soc. Jpn.* **1996**, *65*, 1920–1923 and references therein.

31 Kobayashi, Y.; Fukui, K.; Enoki, T.; Kusakabe, K.; Kaburagi, Y. Edge state on hydro-genterminated graphite edges investigated by scanning tunneling microscopy. *Phys. Rev. B* **2006**, *73*, No. 125415 and references therein.

32 Son, Y.-W.; Cohen, M. L.; Louie, S. G. Half-metallic graphene nanoribbons. *Nature* **2006**, *444*, 347–349.

33 Wassmann, T.; Seitsonen, A. P.; Saitta, A. M.; Lazzeri, M.; Mauri, F. Structure, stability, edge states, and aromaticity of graphene ribbons. *Phys. Rev. Lett.* **2008**, *101*, No. 096402.

34 Hod, O.; Barone, V.; Peralta, J. E.; Scuseria, G. E. Enhanced half-metallicity in edge-oxidized zigzag graphene nanoribbons. *Nano Lett.* **2007**, *7*, 2295–2299.

35 Kan, E. J.; Li, Z. Y.; Yang, J. L.; Hou, J. G. Half-metallicity in edge-modified zigzag graphene nanoribbons. *J. Am. Chem. Soc.* **2008**, *130*, 4224–4225.

36 Stein, S.; Brown, R. Pi-electron properties of large condensed polyaromatic hydrocarbons. *J. Am. Chem. Soc.* **1987**, *109*, 3721–3729.

37 Jiang, D. E.; Sumpter, B. G.; Dai, S. First principles study of magnetism in nanographenes. *J. Chem. Phys.* **2007**, *127*, No. 124703.

38 Fernandez-Rossier, J.; Palacios, J. J. Magnetismin graphene nanoislands. *Phys. Rev. Lett.* **2007**, *99*, No. 177204 and references therein.

39 Hod, O.; Scuseria, G. E. Half-metallic-zigzag carbon nanotube dots. *ACS Nano* **2008**, *2*, 2243–2249 and references therein.

40 Hod, O.; Peralta, J. E.; Scuseria, G. E. First-principles electronic transport calculations in finite elongated systems: A divide and conquer approach. *J. Chem. Phys.* **2006**, *125*, No. 114704.

41 Hod, O.; Peralta, J. E.; Scuseria, G. E. Edge effects in finite elongated graphene nanoribbons. *Phys. Rev. B* **2007**, *76*, No. 233401.

42 Uthaisar, C.; Barone, V.; Peralta, J. E. Lithium adsorption on zigzag graphene nanoribbons. *J. Appl. Phys.* **2009**, *106*, No. 113715.

43 Krepel, D.; Hod O. Lithium adsorption on armchair graphene nanoribbons, *Surf. Sci.* 2010, 10.1016/j.susc.2010.11.019.

44 Hod, O.; Scuseria, G. E. Electromechanical properties of suspended graphene nanoribbons. *Nano Lett.* **2009**, *9*, 2619–2622.

45 Hudspeth, M. A.; Whitman, B. W.; Barone, V.; Peralta, J. E. Electronic properties of the biphenylene sheet and its one-dimensional derivatives. *ACS Nano* **2010**, *4*, 4565–4570.